

Extended Virtual Detector Theory for Strong-Field Atomic Ionization

Xu Wang,* Justin Tian, and J. H. Eberly

Rochester Theory Center and the Department of Physics and Astronomy University of Rochester, Rochester, New York 14627, USA
(Received 29 November 2012; revised manuscript received 18 February 2013; published 14 June 2013)

For time-dependent strong-field atomic ionization a new theoretical approach is described that combines the numerical time-dependent Schrödinger equation (TDSE) and the numerical time-dependent Newtonian equation (TDNE). This approach keeps both the accuracy of quantum calculations and the speed of classical calculations. It does not use approximate tunneling formulas. It is applied to a recent experimental result, and we show its successful comparison to extensive TDSE calculations made under exactly the same conditions.

DOI: [10.1103/PhysRevLett.110.243001](https://doi.org/10.1103/PhysRevLett.110.243001)

PACS numbers: 32.80.Rm, 32.60.+i

Ionization is currently employed as the starting point for essentially all modern strong-field phenomena. These include above-threshold ionization [1], high harmonic generation [2], nonsequential double ionization [3], attosecond pulse generation [4], molecular “self-spectroscopy” [5], attosecond timing [6], etc.

Several high-field theoretical methods are of course well known. Radiative perturbation theory and particularly its Volkov-extended version, the strong field approximation [7–9], have been employed for decades. But for treatment of atomic processes under irradiation with intensities on the order of 1 PW/cm^2 , three other methods have mainly been used to describe and evaluate atomic ionization dynamics. These are (see [10] for a comparative overview) (i) direct numerical solution of the time-dependent Schrödinger equation (TDSE), (ii) direct numerical solution of the time-dependent Newton equation (TDNE), and (iii) a partially classical approach in which the electron is treated classically for the remainder of the laser pulse after assuming that quantum tunneling first releases the electron from its binding potential.

Advantages and disadvantages are obvious for each of these approaches. A direct numerical *ab initio* solution of the TDSE [11] is the most desirable approach. However, the tremendous size of the numerical grid on which the TDSE is to be integrated and the subcycle time resolution needed have proven too resource demanding, particularly for elliptical polarization and circular polarization. Considering that modern experimental data cover a range of intensities and usually use pulses with random phases, the TDSE approach is not usable for almost all tasks of high-field interest.

On the other hand, numerical TDNE integration [12], simulating the atomic system by pure classical mechanics, is very fast, equally *ab initio* and nonperturbative, and requires only modest computing resources. However, it necessarily ignores quantum tunneling, while many experiments are performed well inside the tunneling region (Keldysh parameter $\gamma \ll 1$). It is not a surprise that this

pure classical approach can miss a quantitative match with many high-field experiments.

Regarding approach (iii) [13–16], which has an extensive record of semiquantitative success in conforming to experimental results [10], its tunneling formulas (e.g., [17,18]) contain important initial state parameters that are unavailable to a pure TDNE method. Unfortunately, these formulas become progressively less reliable as the laser field strength approaches or exceeds the overbarrier level [19]. Besides, it is questionable to start the added classical trajectory at a manually assigned tunneling exit point, which can be very far away from the ion core for low intensities and does not even exist for overbarrier intensities.

These merits and drawbacks of the existing approaches motivate a new approach that we present here. It combines an initial stage that obeys quantum principles with a subsequent fast-compute classical stage. This new approach can be regarded as a combination of TDSE via (i) and TDNE via (ii), and it exploits the strength of each. For simplicity we can call it the SENE (Schrödinger equation, Newton equation) approach. But interestingly, the SENE approach is not the same as approach (iii). Instead, SENE fully utilizes (i) throughout and beyond the electron release process, and so avoids the presumption of approach (iii) that dynamical evolution can be treated as beginning abruptly where tunneling ends.

In brief, SENE first solves for the Schrödinger wave function. It starts from the initial atomic quantum state, and continues well beyond electron release. The TDSE part of the computational task can be done quickly using a relatively small numerical grid near the ion core. It is compatible with intensities either below or above the overbarrier level. Then a coherent connection formula uses the TDSE quantum wave function to generate classical trajectories to be carried forward by TDNE calculations. These reliably determine the electron’s subsequent motion under the laser force with very little computational effort. They yield the electron’s momentum components at the end of the pulse,

and importantly fully incorporate final-stage Coulomb effects.

The idea of partitioning the space and treating each partition separately before connecting them coherently in order to reduce the computational loads of numerically tough problems is very attractive. For example, when dealing with a two-electron system, Grobe *et al.* used an algorithm that takes full account of electron-electron interactions in an inner region and neglects them in the outer region [20]. Nikolopoulos *et al.* solve a one-electron TDSE using an R -matrix basis set in an inner region and a finite-difference propagation in the outer region [21]. (A similar but more analytically oriented approach is developed by Torlina and Smirnova [22].) For another example, Tao and Scrinzi have proposed a method that connects an inner region TDSE solution with a Volkov representation in the outer region [23]. Although these methods share the same space-partition concept, they are quite different in their details and in the physical problems to be dealt with.

The innovative core of our method is a coherent “virtual detector” (VD) network that encircles the interaction center, “detecting” the TDSE wave [24]. Further propagation of the electron is not disturbed by this detection because our detectors are imaginary. At each integration time step, the virtual detectors provide numerically the phase and amplitude of the emerging wave function, from which we obtain the momentum associated with the quantum wave at each point on its wave front. The VD technique is able in this way to obtain the exact quantum momentum distribution at a distance sufficiently removed from the ionic core to allow TDNE methods to be safely used for the remainder of the laser pulse.

The necessary formulas are easily constructed. Given a numerical wave function $\Psi(\vec{r}, t)$, the probability flux at the position of a virtual detector (\vec{r}_d) can be calculated:

$$\vec{j}(\vec{r}_d, t) = \frac{i\hbar}{2m} [\Psi(\vec{r}_d, t) \nabla \Psi^*(\vec{r}_d, t) - \text{c.c.}] \quad (1)$$

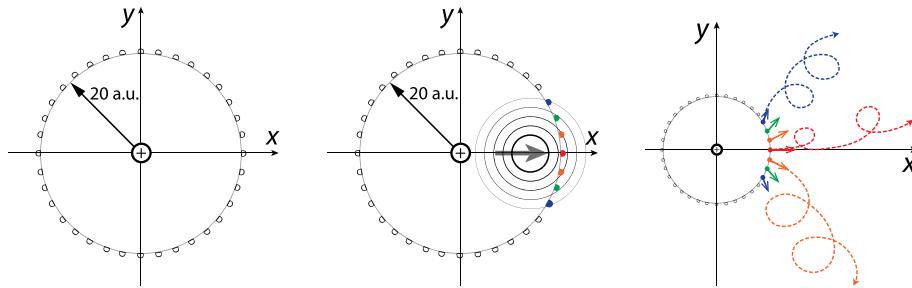


FIG. 1 (color online). Illustration of the new SENE approach. Left: virtual detectors are positioned along a circle of radius 20 a.u. from the atom. The actual number of detectors is much denser (see text). Middle: A TDSE wave packet moving rightward is likely to trigger detectors near the $+x$ axis, with the on-axis detector receiving the strongest signal. Right: Each triggered detector will immediately initiate an electron trajectory at the same position, with its momentum determined by Eq. (2), and a relative weight determined by the probability flux (1). The subsequent motion of each electron trajectory in the remainder of the pulse will be determined by TDNE dynamics.

If one rewrites the wave function in terms of its amplitude and phase $\Psi(\vec{r}, t) = A(\vec{r}, t) \exp[i\phi(\vec{r}, t)]$, and substitutes this expression into Eq. (1), one gets the momentum from the gradient of the phase:

$$\vec{k}(\vec{r}_d, t) \equiv \nabla \phi(\vec{r}_d, t) = \frac{m\vec{j}(\vec{r}_d, t)}{|A(\vec{r}_d, t)|^2}. \quad (2)$$

Detection was the purpose of the original VD application [24], whereas it is used in our method to determine a reliable starting point for outgoing classical trajectories, which will be strongly influenced by both the rest of the laser pulse as well as the ion’s Coulomb attraction. An illustration of the SENE approach is shown in Fig. 1.

We have applied the SENE method to high-intensity single ionization under elliptical polarization, a topic of considerable recent interest [25–28], employing a two-dimensional wave function in the polarization plane. The VDs are arranged evenly along a circle of radius 20 a.u., as illustrated in the left panel of Fig. 1. The actual arrangement is much denser than shown: 400 detectors are placed along this circle [29]. The numerical grid on which the TDSE is integrated is from -51.15 to 51.15 a.u. for each dimension, with a grid spacing of 0.1 a.u. After the quantum wave has been virtually detected and converted to momenta, it is absorbed in a region starting from radius 35.8 a.u., well beyond the virtual detection circle.

The quantum wave function $\Psi(\vec{r}, t)$ at $t = 0$ is found numerically using the imaginary time method with a soft-core model Coulomb potential $V(r) = -1/\sqrt{r^2 + a^2}$ [30]. In the example to be analyzed, ionization was induced by an elliptically polarized laser pulse: $\vec{E}(t) = E_0 f(t) \times [\hat{x} \sin(\omega t + \varphi) + \hat{y} \varepsilon \cos(\omega t + \varphi)]$. Here, $\varepsilon = 0.78$, $\omega = 0.062$ a.u. corresponds to wavelength 740 nm, φ is the carrier-envelope phase (CEP), and $f(t) = \exp(-t^2/2\sigma^2)$ is the Gaussian pulse envelope with duration 7 fs. All parameters are chosen to match recent experimental conditions used for helium [31]. To mimic a random CEP, results from 8 CEPs evenly distributed between $(0, 2\pi)$

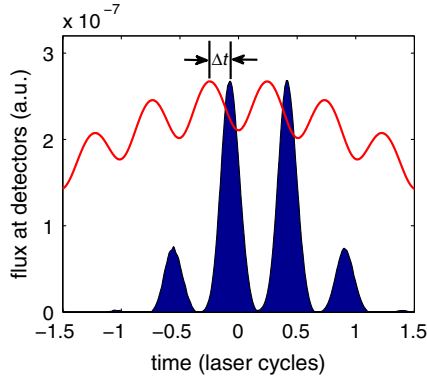


FIG. 2 (color online). Probability flux registered at the detectors versus time (zero is the pulse peak) for the model He atom under intensity 0.4 PW/cm^2 . At each time step, 400 probability flux values are dotted, filling the space below the flux envelope curve. The red curve is the relative laser field strength. Δt is the time delay between emission and detection.

were included. The parameter $a = 0.28 \text{ a.u.}$ is chosen to match the energy of the numerically found ground state to the negative of the empirical ionization potential of helium, which equals 0.9 a.u.

At each time step (1 time step = 0.01 a.u.), the probability flux at the position of each detector is calculated. An example of probability flux versus time is shown in Fig. 2, for intensity 0.4 PW/cm^2 . One sees that substantial probability flux only appears during two cycles at the peak of the pulse. Note that there is a time delay Δt of about 0.2 cycles between the peaks of the pulse and those of the flux. This is the time needed between electron emission and detection, recalling that the detectors are placed 20 a.u. away from the atom. This time delay depends on the laser intensity.

At the same time, each detector that is triggered (above a preset small threshold value) generates a classical trajectory at the same position, with a momentum determined by Eq. (2). This trajectory is given a relative weight equal to the probability flux, determined by Eq. (1). Subsequent motion of this trajectory will be classical, and determined by TDNE integration. The momentum of each trajectory at the end of the pulse will be recorded.

This detector triggering, plus classical trajectory generation, will be repeated at each time step until the end of the pulse. The final momentum distribution is obtained by summing over all classical trajectories with their relative weights.

We have carried out exact numerical TDSE calculations, under precisely the same conditions, and compared results obtained from the SENE approach with them. This means that the TDSE calculation has been performed using the same core potential, the same initial state, and the same laser parameters. The comparison in the end-of-pulse momentum distributions is shown in Fig. 3. One sees that the SENE results reproduce all the relevant features of the TDSE results, such as the orientation angle and the

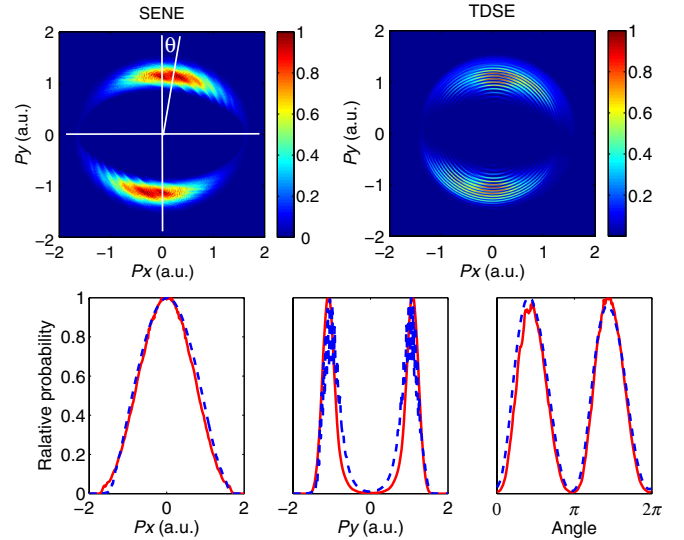


FIG. 3 (color online). Electron momentum distribution obtained from the SENE approach (top left) and from numerical TDSE calculations (top right) under exactly the same conditions. The laser intensity is 0.4 PW/cm^2 . The top two panels have been further compared by projecting onto the P_x axis (bottom left), onto the P_y axis (bottom middle), and by angular scanning from 0 to 2π (bottom right), with the red solid curves for SENE and the blue dashed curves for TDSE. The momentum tilt angle θ has been marked on the first panel as the angle between the P_y axis and the most probable direction of distribution.

projections onto individual axes [32], except for the interference pattern, which originates mainly from wave interference outside the virtual detection circle and cannot be reproduced by the SENE approach.

The results do not depend on the number of detectors, as long as it is not too small. Figure 4 shows the same electron momentum distributions as shown in the first panel of Fig. 3, but using 200 (left) and 800 (right) detectors. No substantial difference is found by using more detectors, expect for a finer resolution.

The results converge as the detection radius is increased. Figure 5 compares the momentum projections for three different detection radii, namely, 15 , 20 , and 30 a.u.

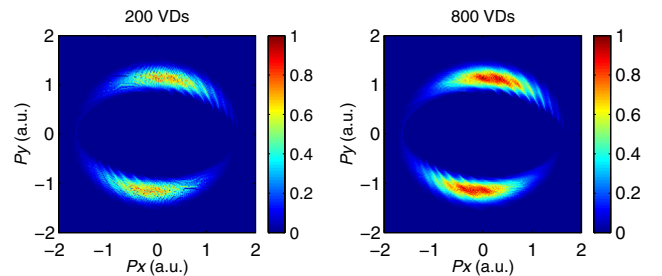


FIG. 4 (color online). The same electron momentum distributions as shown in the first panel of Fig. 3, but using different numbers of virtual detectors. The left panel uses 200 VDs and the right panel uses 800 VDs.

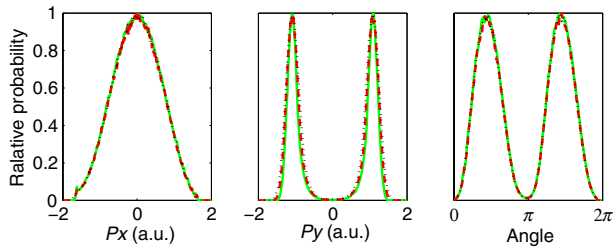


FIG. 5 (color online). Momentum distribution along the P_x direction (left), along the P_y direction (middle), and over the angle from 0 to 2π (right), using three different detection radii, namely, 15 (green), 20 (red), and 30 a.u. (black). They nearly exactly overlap and are not visually distinct.

To avoid contamination from the finite spreading of the ground state, the detection radius should not be too small. But one can see good convergence even for detection radius = 15 a.u.

We can immediately employ the SENE approach in relation to the helium data obtained in the experiments mentioned [31]. Under elliptical polarization the ion-electron Coulomb force prevents the momentum distribution being symmetric against the P_y axis and leads to an angular tilt with respect to this axis, as illustrated in the first panel of Fig. 3 (see [31] for details). Therefore, it is important to take the ion Coulomb potential fully into account. This is automatically done in the SENE approach.

Figure 6 shows the experimental intensity dependence of the tilt angle, as well as the corresponding SENE predictions. Good overall quantitative agreement is evident. Our results, obtained for a single-electron atom, support the conclusion drawn in [31] that for helium, the effect of the remaining electron on the emission of the first electron is negligible.

In summary, we have presented the SENE approach to atomic electron response under high laser fields. This approach coherently joins numerical solutions of TDSE and TDNE types at a radius where the electron has, to excellent approximation, already been freed by fully quantum dynamical evolution. No tunneling event is assumed or

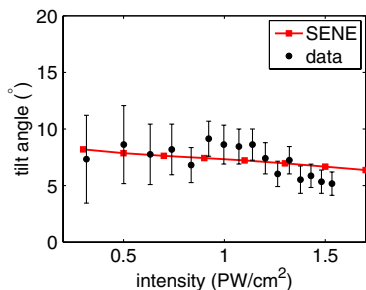


FIG. 6 (color online). Momentum tilt angle as a function of laser intensity. Black dots with error bars are experimental data adapted from Ref. [31]. The red curve is from the new SENE approach.

imposed. The SENE approach starts from the quantum atomic initial state and propagates the wave function on a relatively small numerical grid. Once the outflowing wave reaches the virtual detectors, classical trajectories can safely be initiated. The reliability of classical trajectories beyond the ionization zone has been suggested earlier [33], using masked quantum waves in double ionization calculations. The classical trajectories continue to evolve non-trivially and are followed numerically until the end of the pulse. The weight of each classical trajectory is determined by the probability flux received at the corresponding virtual detector.

The SENE approach has been carefully tested by comparing to numerical TDSE calculations that were made under exactly the same conditions—the same ion core potential, the same initial state, and the same laser parameters. The SENE approach is shown to be able to reproduce all the relevant features of the TDSE results. The results have been checked to be largely independent of the number of virtual detectors and to converge quickly as the detection radius increases.

Finally, because only a small quantum interaction zone is required near the ion core, the SENE approach is not limited to one electron. The extension to two electrons will be used for direct study throughout the ionization process of the effect of electron correlation without imposing a tunneling approximation. We note that standard Volkov waves could be considered to replace the classical TDNE outgoing-electron momenta. However, because the SENE automatically and nonperturbatively includes the effects of final-stage Coulomb forces, it seems likely to remain superior until a Volkov wave function that is fully Coulomb modified (unavailable since 1935) is found.

This research was supported by DOE Grant No. DE-FG02-05ER15713. X.W. acknowledges discussions with Dr. Libin Fu and Dr. Jie Liu at the Institute of Applied Physics and Computational Mathematics in Beijing.

*wangxu@pas.rochester.edu

- [1] H. G. Muller, P. Agostini, and G. Petite, in *Atoms in Intense Laser Fields*, edited by M. Gavrila (Academic Press, New York, 1992).
- [2] A. L'Huillier, L. Lompré, G. Mainfray, and C. Manus, in *Atoms in Intense Laser Fields*, edited by M. Gavrila (Academic Press, New York, 1992).
- [3] W. Becker and H. Rottke, *Contemp. Phys.* **49**, 199 (2008).
- [4] F. Krausz and M. Ivanov, *Rev. Mod. Phys.* **81**, 163 (2009).
- [5] P. B. Corkum, *Phys. Today* **64**, No. 336 (2011).
- [6] P. Eckle, M. Smolarski, P. Schlup, J. Biegert, A. Staudte, M. Schöffler, H. G. Muller, R. Döner, and U. Keller, *Nat. Phys.* **4**, 565 (2008).
- [7] L. V. Keldysh, *Zh. Eksp. Teor. Fiz.* **47**, 1945 (1964) [*Sov. Phys. J.* **20**, 1307 (1965)].
- [8] F. H. M. Faisal, *J. Phys. B* **6**, L89 (1973).

- [9] H. R. Reiss, *Phys. Rev. A* **22**, 1786 (1980).
- [10] W. Becker, X. J. Liu, P. J. Ho, and J. H. Eberly, *Rev. Mod. Phys.* **84**, 1011 (2012).
- [11] J. S. Parker, L. R. Moore, K. J. Meharg, D. Dundas, and K. T. Taylor, *J. Phys. B* **34**, L69 (2001).
- [12] R. Panfili, J. H. Eberly, and S. L. Haan, *Opt. Express* **8**, 431 (2001).
- [13] T. Brabec, M. Yu. Ivanov, and P. B. Corkum, *Phys. Rev. A* **54**, R2551 (1996).
- [14] J. Chen, J. Liu, L. B. Fu, and W. M. Zheng, *Phys. Rev. A* **63**, 011404 (2000).
- [15] G. L. Yudin and M. Yu. Ivanov, *Phys. Rev. A* **63**, 033404 (2001).
- [16] D. F. Ye, X. Liu, and J. Liu, *Phys. Rev. Lett.* **101**, 233003 (2008).
- [17] A. M. Perelomov, V. S. Popov, and M. V. Terent'ev, *Zh. Eksp. Teor. Fiz.* **50**, 1393 (1966) [*Sov. Phys. JETP* **23**, 924 (1966)].
- [18] M. V. Ammosov, N. B. Delone, and V. P. Krainov, *Zh. Eksp. Teor. Fiz.* **91**, 2008 (1986) [*Sov. Phys. JETP* **64**, 1191 (1986)].
- [19] See evaluation in X. M. Tong and C. D. Lin, *J. Phys. B* **38**, 2593 (2005).
- [20] R. Grobe, S. L. Haan, and J. H. Eberly, *Comput. Phys. Commun.* **117**, 200 (1999).
- [21] L. A. A. Nikolopoulos, J. S. Parker, and K. T. Taylor, *Phys. Rev. A* **78**, 063420 (2008).
- [22] L. Torlina and O. Smirnova, *Phys. Rev. A* **86**, 043408 (2012).
- [23] L. Tao and A. Scrinzi, *New J. Phys.* **14**, 013021 (2012).
- [24] Our virtual detectors were inspired by B. Feuerstein and U. Thumm, in *J. Phys. B* **36**, 707 (2003). Ours encircle the real two-dimensional “ionization space” of the electron all the time it is interacting with an elliptically polarized laser pulse. The original Feuerstein-Thumm virtual detectors intercepted ionic fragments of a one-dimensional model dissociation of He_2^+ .
- [25] R. Kopold, D. B. Milošević, and W. Becker, *Phys. Rev. Lett.* **84**, 3831 (2000).
- [26] N. I. Shvetsov-Shilovski, S. P. Goreslavski, S. V. Popruzhenko, and W. Becker, *Phys. Rev. A* **77**, 063405 (2008).
- [27] M. Abu-samha and L. B. Madsen, *Phys. Rev. A* **84**, 023411 (2011).
- [28] N. I. Shvetsov-Shilovski, D. Dimitrovski, and L. B. Madsen, *Phys. Rev. A* **85**, 023428 (2012).
- [29] In general a detector does not fall exactly at a position where a grid point resides. Instead, it is surrounded by four grid points. The value of a physical quantity at the position of the detector is determined by a bicubic interpolation algorithm, using the values and the derivatives of the physical quantity at the surrounding grid points.
- [30] Q. Su and J. H. Eberly, *Phys. Rev. A* **44**, 5997 (1991).
See also J. Javanainen, J. H. Eberly, and Q. Su, *Phys. Rev. A* **38**, 3430 (1988).
- [31] A. N. Pfeiffer, C. Cirelli, M. Smolarski, D. Dimitrovski, M. Abu-samba, L. B. Madsen, and U. Keller, *Nat. Phys.* **8**, 76 (2011).
- [32] For an explanation of the momentum distribution shapes along individual axes, see X. Wang and J. H. Eberly, *Phys. Rev. A* **86**, 013421 (2012).
- [33] S. L. Haan, P. S. Wheeler, R. Panfili, and J. H. Eberly, *Phys. Rev. A* **66**, 061402(R) (2002).